Inorganic Chemistry

Article

pubs.acs.org/IC

AuO: Evolving from Dis- to Comproportionation and Back Again

Andreas Hermann,*[,†] Mariana Derzsi,*[,‡] Wojciech Grochala,[‡] and Roald Hoffmann[§]

[†]Centre for Science at Extreme Conditions and School of Physics and Astronomy, The University of Edinburgh, Peter Guthrie Tait Road, Edinburgh EH9 3FD, United Kingdom

[‡]Centre for New Technologies, University of Warsaw, Żwirki i Wigury 93, 02089 Warsaw, Poland

[§]Department of Chemistry and Chemical Biology, Cornell University, Ithaca, New York 14850, United States

Supporting Information

ABSTRACT: The structural, electronic, and dynamic properties of hypothetical gold(II) oxide (AuO) are studied theoretically, at atmospheric and elevated pressures, with the use of hybrid density functional theory. At p = 1 atm, hypothetical AuO (metastable with respect to the elements) is predicted to crystallize in a new structure type, unique among the late-transition-metal monoxides, with disproportionation of the Au ions to $Au^{I/III}$ and featuring aurophilic interactions. Under pressure, familiar structure types are stabilized: a semiconducting AgO-type structure at ∼2.5 GPa and, with a further increase of the pressure up to ∼80 GPa, an $AuSO_4$-type structure containing Au_2 pairs. Finally, above 105 GPa, distorted NaCl- and CsCl-type $Au^{II}O$ structures dominate, and metallization is predicted at 329 GPa.

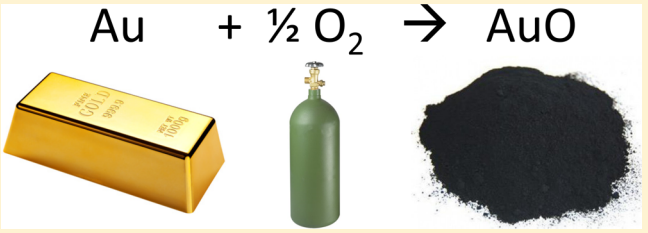

1. INTRODUCTION

When Tutankhamen's tomb was opened, the gold objects in it gleamed as on the day the tomb was sealed. Of course, the reason for this is in the electrochemical series: almost anything in the world will reduce Au ions to metallic Au. Oxides of gold thus do not appear likely candidates for stability; nevertheless, Au_2O_3, with a positive heat of formation, exists and has been studied theoretically together with Au_2O.[1] In this and a subsequent paper, we examine the potential of AuO.

1:1 AuO is not yet known; perhaps that is a good enough reason to study it. There is another motivation for looking at AuO, deriving from the peculiarities of the group 11 oxides above gold.[2] AgO is a "frozen" mixed-valence compound with disproportionated Ag^{I} and Ag^{III} ions, linearly and square-planar coordinated, respectively. In CuO, Cu, which usually takes on oxidation states 2+ and 1+, is clearly Cu^{II}.[3] In the high-T_c cuprates, that oxidation state can be tuned by substitution, up and down from 2+. Also, there is a hint that the oxidation state fluctuations $Cu^{I} \leftrightarrow Cu^{II} \leftrightarrow Cu^{III}$ play a role in the high T_c in these compounds.[4,5]

The question is then not only does AuO potentially exist (perhaps under pressure) but also what will the Au ions do in such a compound: will they be in oxidation state 2+, or will they disproportionate to 1+ and 3+, as one finds in AgO? Also, what will its conducting properties be? Pressure is another variable that has been used to tune the transition to superconductivity in the cuprates,[6] and so it will be instructive to play with this variable in AuO.

2. COMPUTATIONAL METHODOLOGY

The *VASP* package was used to perform density functional theory (DFT) calculations, using the Perdew–Burke–Ernzerhof (PBE), the PBEsol, and the hybrid HSE06 exchange-correlation functionals and different projector-augmented-wave (PAW) "frozen-core" choices with corresponding plane-wave basis sets.[7−12] To uncover enthalpically relevant structures for AuO, we performed evolutionary structure searches with the *XtalOpt* package.[13] The structure search approach, which complements chemical or physical intuition, has been used successfully, particularly to study high-pressure phases of compounds.[14−18] Here, structure searches with four formula units per cell were performed at pressures of 1 atm and 100, 200, 300, and 400 GPa using the PBE functional with "soft" PAW data sets and a plane-wave cutoff of 300 eV. Additional pressure points were scrutinized only for selected structures, those that were relevant to phase transitions occurring in given pressure regions. Structural candidates were then reoptimized across the entire pressure range with the PBEsol functional and "hard" PAW data sets (including 6 and 17 valence electrons for O and Au atoms, respectively) and a corresponding plane-wave cutoff of 800 eV. The PBEsol functional is a reparameterization of the PBE functional suitable for solids and generally gives better agreement with experiment regarding lattice constants, elastic properties, and (for compounds with ionic bonding components) cohesive energies.[19,20]

Structures were optimized until the remaining forces were below 1 meV/Å. Brillouin zone integrations were performed on regular k-point grids with a linear spacing of 0.16 $Å^{-1}$. Electronic band structures and density-of-state (DOS) calculations were carried out with both the PBEsol and hybrid HSE06 functionals, using geometries optimized at the respective level of theory. Crystal structure optimizations using the CPU-demanding hybrid HSE06 functional were done with a plane-

Received: November 2, 2015
Published: January 21, 2016

DOI: 10.1021/acs.inorgchem.5b02528
Inorg. Chem. 2016, 55, 1278−1286

wave cutoff of 500 eV and a k spacing of 0.35 Å^{-1}. Additionally, enthalpies and electronic DOSs were recalculated with a denser k spacing of 0.24 Å^{-1} for structures optimized with the hybrid HSE06 functional. The pressures of the phase transitions at the HSE06 level were obtained using linear interpolation between adjacent computed pressure values.

Normal modes at the zone center were calculated for the most important structures using *VASP*.[7,8] Vibrational zero point energy was found to have a negligible effect on the stability and was not considered. Every structure examined in this paper is a ground-state static phase; i.e., there is no consideration of the temperature-mediated influence of entropy on the structural stability.

3. RESULTS AND DISCUSSION

AuO at Atmospheric Pressure. Our structure searches at P = 1 atm resulted in a variety of candidate structures; see Figure 1. Among those are known metal oxide structure types

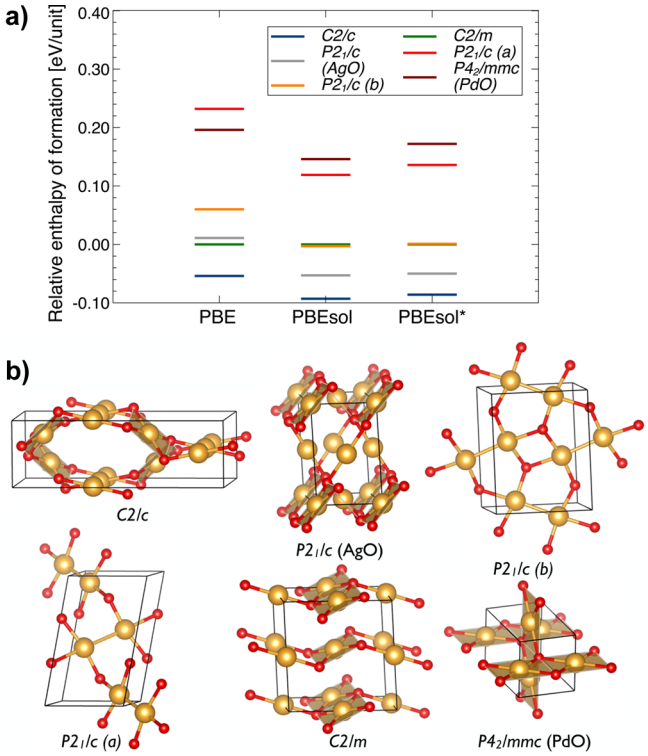

Figure 1. Enthalpies of formation (top, relative to the $C2/m$ structure) and structures (bottom) of selected low-energy AuO phases at atmospheric pressure as obtained from crystal structure prediction. The functionals used are indicated. PBEsol* refers to using "hard" small-core PAW data sets. Au (O) atoms are shown as golden (red) spheres. Structures are from PBEsol* optimization.

(more on those below) and others that are new. In particular, we find AuO to be most stable in a monoclinic $C2/c$ structure, a new structure type not seen in other transition-metal oxides. The structure does, however, recite features of the CuO, mixed-valence AgO ($Ag^{1+}Ag^{3+}O_2$), and PdO structures. The difference between these and the AuO structure is perhaps not too surprising, given the so-called "aurophilic interactions" between the metal atoms of the latter;[21−23] more on this will follow anon.

CuO crystallizes in a monoclinic structure, space group $C2/c$, where all Cu atoms are identical and connected in a nearly planar geometry to four O atoms; see Figure 2.[24,25] Although sharing a common space group with our best AuO structure, the CuO geometry differs in detail. In it, each O atom is, in turn, shared between four Cu atoms. Overall, the structure has doubly bridged chains of Cu atoms running through the lattice, which alternate direction along the c axis, and are not quite orthogonal to each other. The Cu atoms, being Cu^{II}, have a d^9 electronic configuration, which explains their departure from octahedral coordination (in a parent NaCl structure[26]) to a square-planar one. Copper(II) complexes sometimes also show a distortion from square-planar to tetrahedral coordination, as in $CuCl_4^{2-}$.[27,28] The CuO structure is a distorted variant of the tetragonal PdO structure (space group $P4_2/mmc$), where each Pd atom is ideally square-rectangular-coordinated and the bridged chains of Pd atoms are orthogonal within the ab plane.[29,30] In Figure 2, this relationship between CuO and PdO, but also with AgO and the proposed AuO structure, is shown.

One of the known AgO polymorphs also crystallizes in a monoclinic structure (the other being tetragonal), space group $P2_1/c$. However, it prefers a clearly disproportionated structure, with linear coordinated Ag^{I} atoms (electronic configuration d^{10}) as well as square-planar Ag^{III} atoms (electronic configuration d^8).[31] The actual structural difference between CuO and $P2_1/c$ AgO is relatively small, and both deviate little from the PdO structure;[32] see Figure 2. In fact, both phases can be seen, together with PdO and other late-transition-metal oxides, as deformations of the rock-salt structure; the differences between them may be explained in terms of coordination chemistry and collective Jahn−Teller effects.[26,33]

For AuO, all of the structures mentioned above were found as local minima during the evolutionary structure search, with the AgO structure being the most stable of these. This energetic order is not surprising because one might have expected a disproportionated structure for AuO. The global minimum ($C2/c$), however, is 36 meV/formula unit more stable than the AgO structure and is shown in both Figures 1 and 2 (see the Supporting Information (SI) for crystallographic information on this and all other relevant AuO phases discussed throughout). Through a slightly different coordination network (compared to AgO), linear −Au−Au−Au− chains form within the structure (see Figure 2). Along those chains, Au^{I}−Au^{I} separations are 2.78 Å. This separation is short and much shorter than the Au^{III}−Au^{III} separations (3.36 Å) in the same structure, as well as Ag^{I}−Ag^{I} and Ag^{III}−Ag^{III} (both 3.26 Å) in AgO. Linear chains of Au atoms have been found in the crystal structure of inorganic gold polymeric complexes, albeit with longer Au−Au distances of 2.91−3.11 Å.[34] Just like in PdO, CuO, and AgO, this structure for AuO can be traced back to a distorted rock-salt structure, although with larger distortions than those for the other compounds. In analogy with our earlier work,[26] the corresponding matrix transformation relative to the rock-salt archetype and atomic displacements from it are given in the SI.

We thus identify the interaction between the Au^{I} ions as an aurophilic interaction. Originally traced to d_{z^2} sp mixing,[35−38] this closed shell−closed shell d^{10}−d^{10} interaction has been reassigned to exchange interactions beyond the Hartree−Fock level, essentially a strong correlation−dispersion interaction with a significant relativistic contribution.[39−41] The nominal oxidation state of the Au ions can be corroborated with partial charges from a Bader analysis of the total charge density, which are +0.47 for Au^{I} and +1.12 for Au^{III} and, consequently, −0.79 for the O ions (all numbers from the PBEsol functional). We are well aware that formal oxidation states are a convenient fiction, and the relationship of calculated charges—by whatever

DOI: 10.1021/acs.inorgchem.5b02528
Inorg. Chem. 2016, 55, 1278−1286

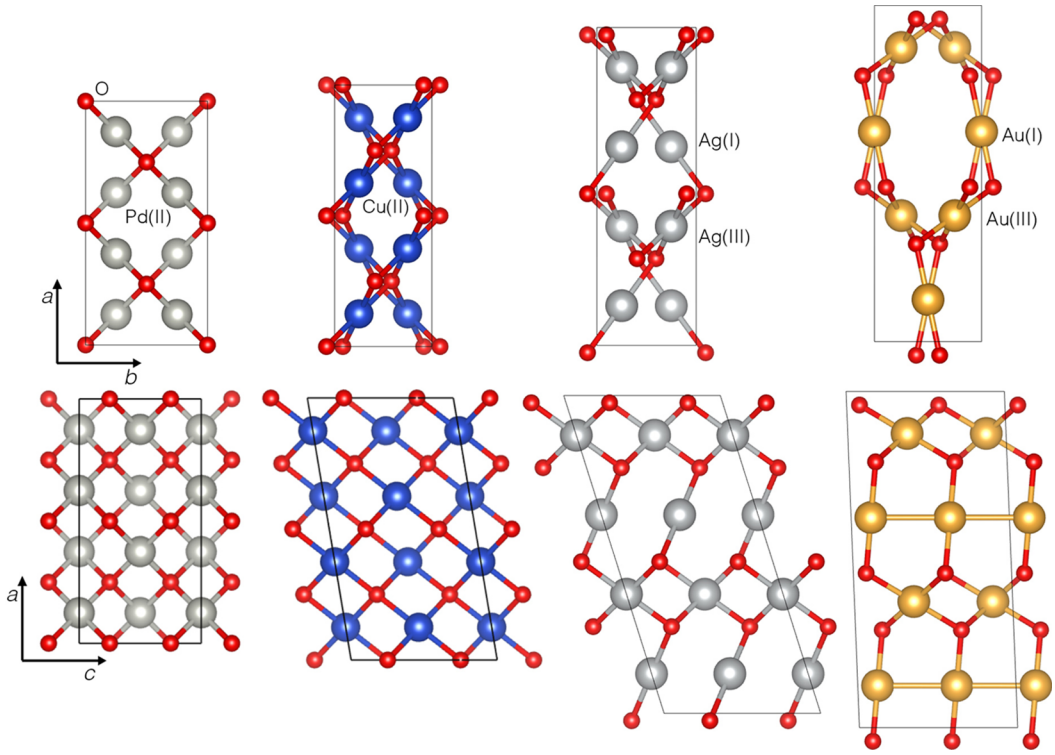

Figure 2. Crystal structures of some of the late-transition-metal oxides at atmospheric pressure, as seen along the *c* axis (top) and *b* axis (bottom). From left: PdO, $P4_2/mmc$ structure; CuO, $C2/c$ structure; AgO, $P2_1/c$ structure; proposed AuO, $C2/c$ structure. In AuO, proposed aurophilic Au^I–Au^I interactions are drawn as gold lines. All structures are drawn to the same scale and were optimized with the PBEsol functional.

uniquely defined but arbitrary method one uses to calculate them—to oxidation states is muted.

The mixed-valence character of AuO is further evident from the electronic DOSs (see Figure 3). The electronic structure is

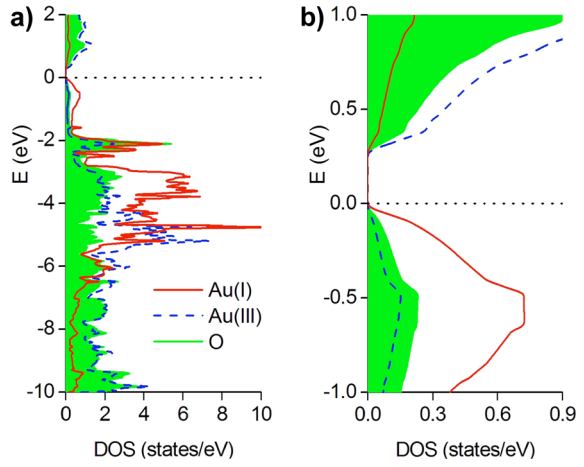

Figure 3. Atomic projections of electronic DOSs of $C2/c$ AuO at ambient pressure (from HSE06): (left) −10 to +2 eV energy range; (right) focused around the band-gap region.

dominated by Au 5d states, with O 2p states mixing in. However, the partial DOS for Au^I is substantially different from that of Au^{III} in the broad energy window. One significant difference is that Au^{III} states are, on average, at larger binding energies than those of Au^I. This should be expected based on both formal oxidation states as well as Bader charges.

It will be noted that the Au^I states make up most of the top of the valence band, while the Au^{III} states predominate in the conduction band. This, too, is anticipated for a classic mixed-valence system, for which intervalence charge-transfer excitations should contribute most to the electronic conductivity. For AuO, the valence band is composed mostly of the lone pairs at the Au^I cation (a combination of $5d_{x^2-y^2}$ and $5d_{z^2}$ and relativistically stabilized 6s orbitals), while the conduction band is made of empty Au−O antibonding $5d_{x^2-y^2}$/6s states of Au^{III}. AuO, i.e., $Au^IAu^{III}O_2$, should thus be not much different in this respect from AgO, a prototypical d^{10}/d^8 frozen valence system.[42]

The aurophilic interactions directly influence the electronic properties of AuO in the generalized gradient approximation (GGA) description, rendering this system metallic at P = 1 atm (cf. the SI). Using the hybrid HSE06 functional, which includes screened exchange interaction, AuO has a small band gap of 0.27 eV (see Figure 3). This band gap is much smaller than those of Si (1.11 eV), Ge (0.67 eV), and PbS (0.41 eV) and comparable with that of PbTe (0.31 eV). If prepared (more on its stability below), AuO would thus be a very narrow-band-gap semiconductor. The closest (in enthalpy) metastable structural alternative to the $C2/c$ structure, the $P2_1/c$ AgO-type structure, lacks aurophilic interactions and has (at the HSE06 level of theory) a band gap of about 0.98 eV (or 0.2 eV at the PBEsol level of theory). The calculated band gap of AuO in the $P2_1/c$ AgO-type structure is very similar to that computed recently for related AgO in the same structure type (0.94 eV[43]).

In our calculations, we find AuO to be unstable with respect to decomposition into Au + $^1/_2O_2$ by 89 meV/unit at the HSE06 level of theory but stable by 59 meV/unit at the PBEsol level of theory. Note that DFT functionals, hybrid or otherwise, have problems describing the magnetic ground state of solid oxygen,[44,45] and these formation enthalpies are thus less certain than one would like. A synthesizable system in the solid state

DOI: 10.1021/acs.inorgchem.5b02528
Inorg. Chem. 2016, 55, 1278−1286

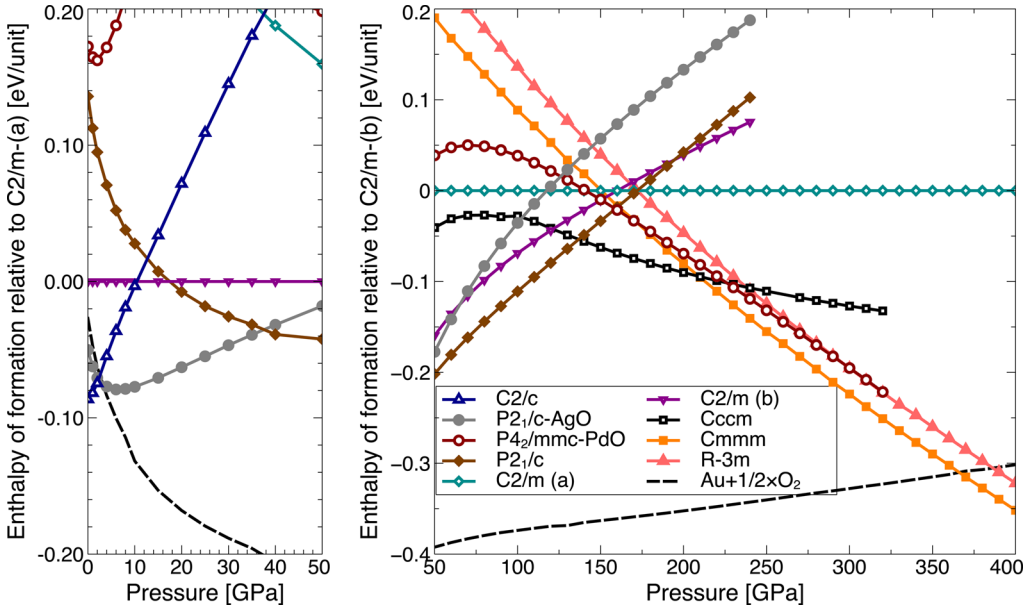

Figure 4. Relative enthalpies of formation for AuO structures as a function of the pressure, from PBEsol calculations: (left) low-pressure regime below 50 GPa; (right) high-pressure regime above 50 GPa. Note the different enthalpy scales and different baseline structures. The enthalpy of the elements, Au + $^1/_2O_2$, is shown as the dashed line. See the SI for the volume changes with pressure for the most relevant structures.

should also exhibit dynamic stability; i.e., all of its phonon frequencies must be real. We have calculated phonon modes at the zone center with both PBEsol and HSE06. All phonon modes are real (cf. the SI), attesting to the dynamic stability of the *C*2/*c* polymorph.

AuO under Pressure: First, an AgO Structure. The ground-state structure of AuO at P = 1 atm is overall rather open, having quite wide "channels" along the *c* axis (clearly seen in Figure 2). This leads to a volume per formula unit of ∼31.1 Å^3, which agrees with an estimated volume of 30.3−33.1 Å^3, as calculated from the difference of the corresponding volumes of $AuSO_4$ (88.25 Å^3)[46] and SO_3 (55.12−57.96 Å^3).[47,48] When external pressure is applied, phase transitions to more compact, close-packed structures should be expected. Indeed, this is the case. We find with the HSE06 functional that at a mere p = 0.8 GPa (2.5 GPa with PBEsol) the $P2_1/c$ AgO-type structure becomes more stable; see Figure 4. This structure, discussed above, also contains Au^I and Au^{III} ions, but the directions of the linear O−Au^I−O units allow for more compact packing: at the transition pressure, the unit cell of the $P2_1/c$ AgO structure is 9 vol % smaller than that of the *C*2/*c* structure (7 vol % PBEsol).

Note that an increase in pressure also leads to a rapid stabilization of the decomposition product, indicated as the dashed line in Figure 4. Eventually, at very high pressures exceeding 370 GPa, we find AuO becoming stable again compared to the elements.

Higher Pressure: Comproportionation in the $AuSO_4$ Structure. At p = 82 GPa (37 GPa with PBEsol), another $P2_1/c$ structure becomes the most stable phase of AuO. The structure (see Figure 5) is distinguished in two ways: First, this is the pressure of comproportionation, where all Au atoms attain identical coordination environments and are thus formally in the Au^{II} oxidation state. A Bader charge analysis[49] with the PBEsol functional assigns at p = 80 GPa a partial charge of +0.84e to the Au^{II} ion, very close to the mean of the Au^I/Au^{III} charges (+0.85e, see above). Second, it features Au−Au dimer units bound by what appears to be a two-electron chemical bond and not just an aurophilic interaction: the Au^{II} atoms are square-planar-coordinated, leaving one electron pair for the Au−Au bond; the separation (2.42 Å at 80 GPa) is much shorter than a typical aurophilic separation (or 2.67 Å in face-centered-cubic Au metal); the bond is significantly less compressible (it is 2.66 Å at 1 atm) than an aurophilic interaction. Distinct Au_2O_6 units can then be perceived in this structure, with all O atoms shared between adjacent units. Salts of M_2L_6 with direct M−M bonds, where M is a group 10 metal, have been characterized; in those, the square-planar-coordinated ML_3 units are usually perpendicular to each other,[50−53] unless bridging groups enforce an overall planar geometry.[54−57]

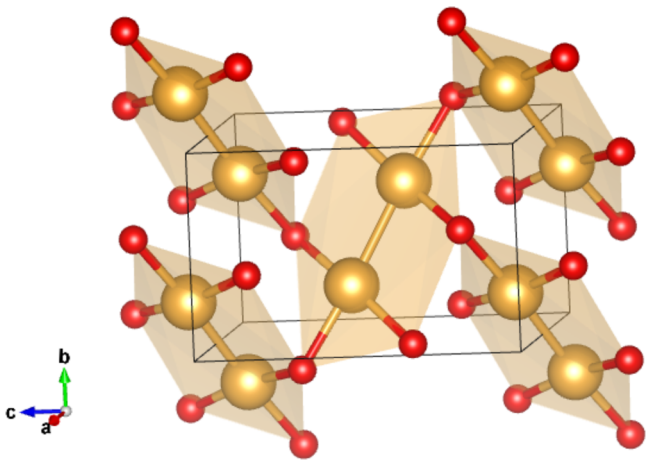

Figure 5. High-pressure $P2_1/c$ phase of AuO, shown here at p = 82 GPa (from the PBEsol functional). Au_2O_6 units are emphasized.

In our recent work, we emphasized structural similarities between late-transition-metal oxides and their respective sulfates, with the O^{2-} and $(SO_4)^{2-}$ sublattices being close to each other.[26] A plausible structure for AuO could then be gained from known $AuSO_4$ by substitution SO_4 → O. The $P2_1/c$ structure discussed here is identical with the most stable AuO structure obtained from such a substitutional ansatz.[58] The relationship between oxide and sulfate found in other late

DOI: 10.1021/acs.inorgchem.5b02528
Inorg. Chem. 2016, 55, 1278−1286

transition metals thus carries over to the case of gold as well but is restricted to a certain range of elevated pressure.

Still Higher Pressures: Relatives to the NaCl and CsCl Structures. At even higher pressure, around p = 105 GPa (137 GPa with PBEsol), more close-packed structures are stabilized, and the Au_2 dimer feature becomes unfavorable. The most stable structure between 105 and 329 GPa is orthorhombic, of *Cccm* symmetry, and features square-planar-coordinated Au^{III} ions alternating with square nets of nonclassical cubic-coordinated Au^{I} ions; see Figure 6. We see here the appearance of the ionic CsCl B2 structure: the square-planar-coordinated Au^{III} ions, together with the O atoms, form a severely distorted B2 sublattice (so we have effectively 4 + 4 coordination), whereas the square-net Au^{I} ions, together with the O atoms, form an almost perfect B2 sublattice. The coordination polyhedra of the two different Au sites, shown in Figure 6, illustrate these two different environments. This structural interpretation is corroborated by a Bader partial charge analysis: at p = 200 GPa, the Au^{I}/Au^{III} sites have a partial charge of +0.69e/+1.03, with a corresponding partial oxygen charge of −0.86e. Thus, AuO is again disproportionated in this pressure range.

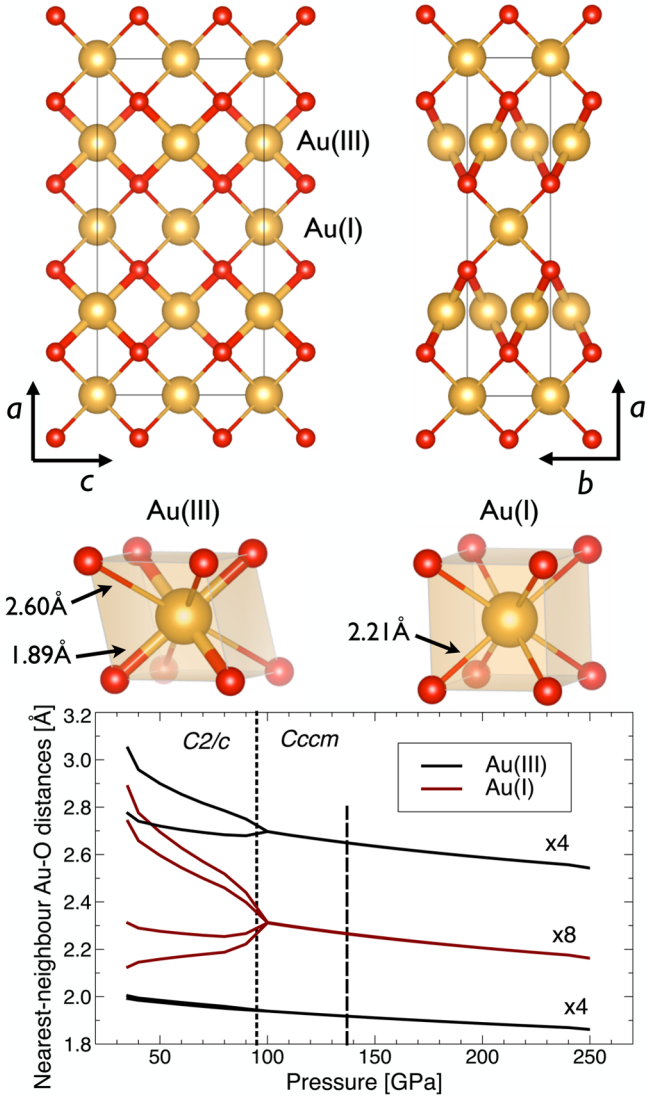

Figure 6. Structural features of *Cccm* AuO at p = 200 GPa, optimized with the PBEsol functional. From top to bottom: two views of the structure, with different Au sites labeled, the coordination polyhedra of the Au sites, with nearest-neighbor Au−O distances indicated, and the evolution of those Au−O distances (with 4- or 8-fold degeneracy pointed out) as a function of the pressure. Below 95 GPa, the *Cccm* structure optimizes with PBEsol to a lower-symmetry metastable *C*2/*c* structure; above 137 GPa, the *Cccm* structure is stable.

At pressures above p = 329 GPa (210 GPa with PBEsol), comproportionated close-packed orthorhombic and rhombohedral structures are most stable. Enthalpies of formation of the latter are shown in Figure 4 and the respective structures themselves in Figure 7. The lowest-enthalpy *Cmmm* structure is

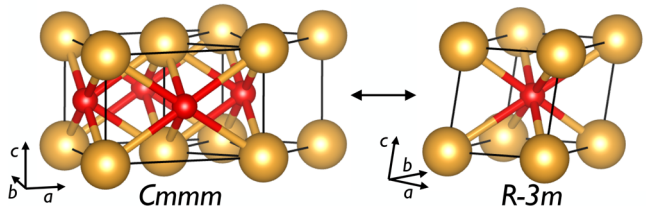

Figure 7. High-pressure *Cmmm* and $R\bar{3}m$ phases of AuO shown at 330 GPa. The primitive unit cell of *Cmmm* (with Z = 1) is also indicated.

an orthorhombic compression (for its primitive cell at p = 330 GPa: $a/c = b/c$ = 0.955) of the B2 (CsCl) structure, and the $R\bar{3}m$ structure is on the rhombohedral structural transition (Buerger[59]) path connecting the B1 and B2 structures (at p = 330 GPa: α = 83.1°, where α = 90° corresponds to the B2 structure and α = 60° to the B1 structure); see Figure 8. Moreover, the *Cmmm* structure is an intermediate along the more sophisticated B1−B2 transition paths suggested by Watanabe et al.[60] and Tolédano et al.[61] and also the global minimum along both those paths (see the SI for the corresponding potential energy surfaces). At p = 365 GPa (with PBEsol), the *Cmmm* structure becomes stable against decomposition into the elements; see Figure 4. With the HSE06 functional, this stabilization is found at slightly lower pressures, just above 300 GPa, and still in the stability region of the *Cccm* structure.

The $R\bar{3}m$ and *Cmmm* structures are connected through a monoclinic distortion, as shown in Figure 8. The monoclinic distortion of the *Cmmm* structure, which involves sliding of adjacent Au layers along the *c* axis, results in a set of monoclinic *C*2/*m* structures. This distortion eventually results in the rhombohedral $R\bar{3}m$ structure with $\gamma = \beta = \alpha$ = 83.1° (at p = 330 GPa). The latter (where every Au atom has "6 + 2" coordination in O) is less favorable than the *Cmmm* structure, where Au−O coordination is "4 + 4", thus allowing a close packing while keeping square-planar Au coordination intact. However, the $R\bar{3}m$ structure is a local minimum along the transition path from the NaCl B1 structure to the CsCl B2 structure (where Au−O coordination is 6 and 8, respectively).

It is remarkable that even at pressures as large as 350 GPa, the d^9 cation, Au^{II} here, preserves its preference for the square-planar geometry. This may be viewed as a manifestation of pronounced steric activity of the $5d_{z^2}$ lone pair, which is well-known for both gold(III)[62] and gold(II) compounds[63] at 1 atm.

It seems that there is use for chemical intuition, here preferences in the coordination environment as a function of the electron count, applied to matter compressed to 3.5 million atm.

DOI: 10.1021/acs.inorgchem.5b02528
Inorg. Chem. 2016, 55, 1278−1286

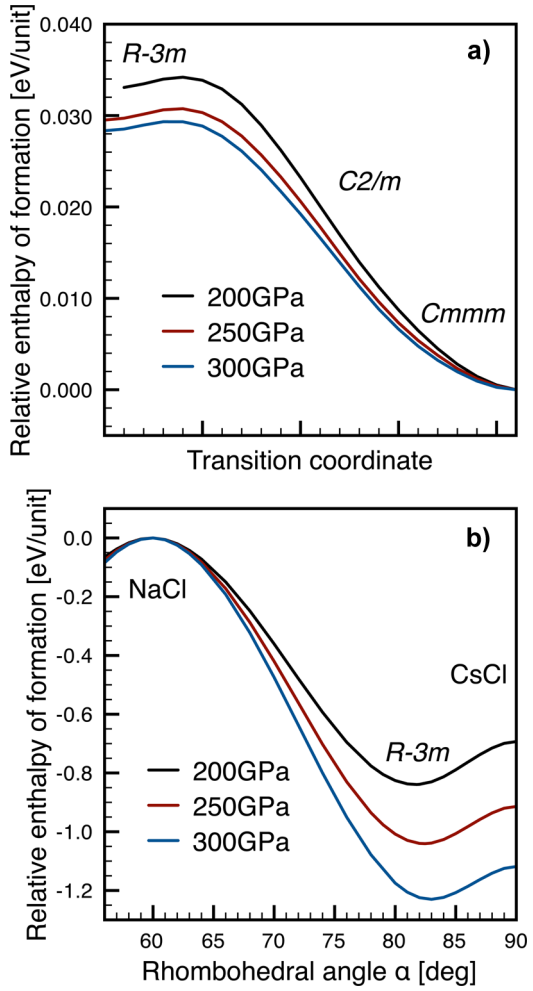

Figure 8. Top: Continuous transition between the lowest-enthalpy high-pressure structures, $R\bar{3}m$ and *Cmmm*. Bottom: Continuous transition between the NaCl B1 and CsCl B2 structures along the Buerger path, with the $R\bar{3}m$ structure as the local minimum. All enthalpies obtained from PBEsol calculations.

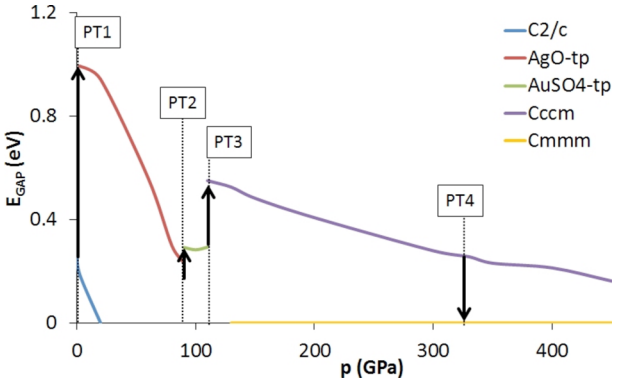

Figure 9. Progression of the fundamental electronic band gap for various polymorphic forms of AuO. The stability limits of various polymorphs have been marked, where "PT" denotes the various phase transitions. All calculations here are with the HSE06 functional. Note that the PBEsol functional predicts all these structures to be metallic across the entire pressure range.

Evolution of the Band Gap at the Fermi Level of AuO with External Pressure. Evolution of the fundamental electronic band gap of AuO as a function of the pressure is of interest. We have studied the electronic structure of various crystalline forms of AuO up to 400 GPa (see Figures 9 and 10 and the SI for DOS calculated at the PBEsol level of theory).

As already mentioned, the *C*2/*c* polymorph, which is the lowest-energy structure at 1 atm, has a small band gap of 0.27 eV calculated with the hybrid HSE06 functional (but artificially closed in the PBEsol calculations). It might be expected that such a small band gap could be closed rather easily with pressure, and indeed, the gap is computed to be null at pressures below 20 GPa. However, as already discussed, a phase transition at 0.8 GPa to the $P2_1/c$ AgO structure type should take place. This new polymorph has a band gap of ∼1.0 eV at the phase transition, and its gap is not as easily closed as that of its predecessor; it maintains a band gap throughout its region of stability; see Figure 9. A similar mechanism for preserving a quasi-gap in compressed AgO[43] brings to mind Pearson's Maximum Hardness Principle.[64]

The next phase transition related to comproportionation (to the $AuSO_4$-type structure) is computed to take place at 82 GPa. At this pressure, the band gap for the $P2_1/c$ AgO structure is ∼0.20 eV, while the value for the resulting $AuSO_4$ polytype is very similar, ∼0.28 eV. Interestingly, the band gap of this polymorph tends to be quite constant up to 100 GPa and then even begins to slightly increase with pressure rather than decrease (Figure 9). The next phase transition, connected with subsequent disproportionation, has been predicted to occur at 105 GPa. The resulting *Cccm* polytype turns out to have a much larger band gap than its predecessor, over 0.5 eV at the phase transition. We see the Maximum Hardness Principle at work again despite considerable compression. This new structure also maintains a finite (hybrid DFT) band gap throughout its stability range and even beyond 450 GPa.

At 329 GPa, the *pV* term related to packing of the crystal structure, which is a key factor influencing the stability at high pressure, drives the transition from the *Cccm* phase to the *Cmmm* phase. The *Cccm* polytype at this pressure has a band gap of 0.26 eV, comparable to that of the ambient-pressure *C*2/*c* form. This example is instructive for realizing how stubbornly AuO resists metallization to 329 GPa. At this pressure, the band gap finally closes for the thermodynamically preferred *Cmmm* type, which is the first unambiguously metallic AuO phase. It is only at this immense pressure that the electronic arguments related to Pearson's hardness no longer apply and close(st) packing has its say.

The electronic DOS for the *Cmmm* structure at 350 GPa (Figure 10) shows the expected splitting of the Au 5d bands, with (in this case of square-planar coordination) a significant stabilization of the in-plane d_{xz} and d_{yz} orbitals. Still, significant band overlap makes this phase a relatively good metal, at both levels of theory considered (HSE06 and PBEsol). Interestingly, this polytype is structurally two-dimensional, with an appreciable difference between intrasheet and intersheet Au−O separations of ∼15% (at 330 GPa); this renders the *Cmmm* structure a 2D metal, as is evident also from inspection of its band structure (cf. Figure SI 5 in the SI). The comproportionated *Cmmm* structure realizes a genuine $Au^{II}O$ formulation and should be the lowest-enthalpy polymorph of AuO up to 400 eV, where our scrutiny ends.

AuO should resist metallization up to pressures beyond the metallization pressure of O_2 alone (>100 GPa).[65] It should be stressed here that the semilocal PBEsol functional is incapable of predicting the finite band gap for all polymorphic forms of AuO except the *Cmmm* one. This well-known deficiency of

DOI: 10.1021/acs.inorgchem.5b02528
Inorg. Chem. 2016, 55, 1278−1286

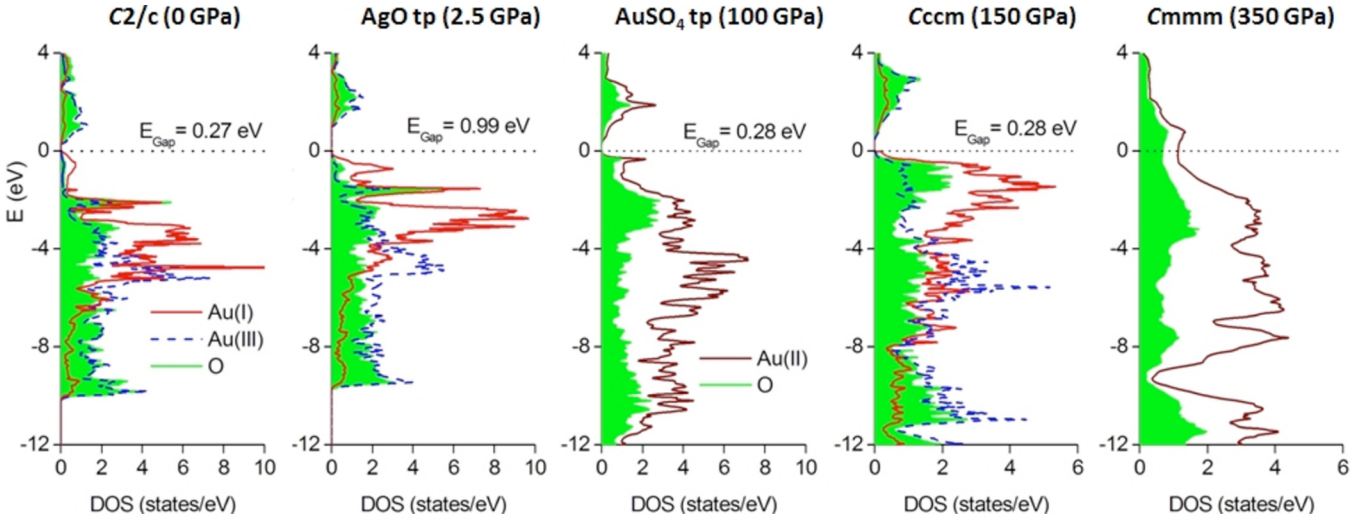

Figure 10. Partial DOS (HSE06) for various polymorphic forms of AuO at pressures selected from the regions of their thermodynamic stability.

standard DFT methods should discourage researchers from applying it to predictions of the electronic structure of novel compounds;[66] sadly, common practice in the trade shows that it does not.

Stability Again. In Figure 4, we saw that AuO remained *unstable* relative to the elements from ∼2 GPa up to ∼370 GPa. That was a result obtained with the PBEsol functional. When the calculations are repeated with a hybrid HSE06 functional, one obtains somewhat different results, as shown in Table 1;

Table 1. Comparison of Enthalpies Concerning the Au + $^1/_2O_2$ → AuO Reaction[a]

Enthalpies per Formula Unit (HSE06)			
GPa	AuO	Au + $^1/_2O_2$	ΔH/eV
0	−12.444	**−12.533**	−0.089
100	1.531	**1.415**	+0.116
200	12.480	**12.419**	+0.061
300	22.334	**22.328**	+0.006
400	**31.405**	31.503	**−0.098**
450	**35.725**	35.878	**−0.153**

[a]Cubic gold was found to be more stable than the hexagonal form of gold at all pressures. Concerning oxygen, the α form was considered at 0 GPa and the ε form at elevated pressures.

AuO is then unstable relative to the elements for pressures below 305 GPa. The discrepancy between both methods is substantial in both the low- and high-p regimes, and it emphasizes shortcomings of standard DFT in dealing with strongly correlated systems. However, the energetic metastability of AuO at 1 atm in the ground state (it would be unstable with respect to O_2 formation at ambient conditions) and its reentrant stability at pressures exceeding 300 GPa (assisted by its dynamic stability; cf. the SI) jointly suggest that this compound might constitute a viable synthesis target, especially at low temperatures.

4. CONCLUSIONS

AuO is an as-yet-unsynthesized oxide of a noble metal. With an ionic radius of Au^{II} of ca. 1.33 Å[67] and an ionic radius of the oxide dianion of 1.24−1.28 Å and using Pauling's rules, one might expect AuO to adopt the CsCl structure. However, the formal d^9 half-occupation of the atomic 5d orbital of gold, close to the shell filling, is associated with partial occupation of Au−O antibonding orbitals and leads to strong vibronic effects, which result in structural distortions. Moreover, the possibility of disproportionation to Au^{III} d^8 and Au^{I} d^{10} adds to the complexity.

At p = 1 atm, we predict for AuO a disproportionated structure (in that aspect like AgO but differing from CuO) with discrete square-planar Au^{III} and linear Au^{I} ions. The calculated *C*-centered monoclinic structure is characterized by aurophilic interactions between the Au^{I} ions but is quite open. Standard DFT-GGA predicts it to be metallic, but using hybrid functionals, we find it should have a small band gap of ∼0.27 eV. As such, the compound should be black and possibly very reactive (in the sense of reaction kinetics). The calculated phonon spectrum of AuO shows no imaginary modes, and thus this phase should be dynamically stable, and potentially observable.

Elevation of the pressure to a mere 0.8 GPa leads to a more compact AgO-type primitive monoclinic structure that is semiconducting. At p ∼ 82 GPa, comproportionation occurs, in a remarkable $AuSO_4$-related structure that features Au_2O_6 units, with genuine Au^{II}−Au^{II} bonding and familiar square-planar coordination of Au^{II} cations.[62,63] All Au atoms are equivalent in this phase. At still higher pressures, above p = 105 GPa, we predict a transition of the oxide to the *C*-centered orthorhombic polytype, which is again disproportionated and still semiconducting. This *Cccm* polymorph is stable up to ∼329 GPa; it features classical square-planar $Au^{III}O_4$ and dumbbell $Au^{I}O_2$ units. Notably, the geometrical preferences of Au cations at this pressure resemble those exhibited at 1 atm.

The phase transition at ∼329 GPa leads to distorted NaCl- and CsCl-type structures, with metallization occurring at the onset of the stability of the orthorhombic *Cmmm* phase. Thus, metallization of AuO is predicted to occur at much higher pressure than that of related AgO (∼45 GPa).[43] AuO is again comproportionated up to 400 GPa, the highest pressure studied here.

The stability of AuO as a function of the pressure and with respect to elements as well as other gold oxides is naturally of interest. This is actually a very rich topic because Au exhibits a broad range of oxidation states from 1− to 5+ (even with 7+ sometimes discussed[68,69]), which gives rise to a multitude of stoichiometries, including mixed-valence compounds and

DOI: 10.1021/acs.inorgchem.5b02528
Inorg. Chem. 2016, 55, 1278−1286

subvalent phases.[70,71] Moreover, many oxidation states of Au are prone to disproportionation,[72] which results in structural complexity (just like for AuO studied here). Last but not least, the correct treatment of disproportionated compounds usually necessitates the use of hybrid DFT methods, which are very time-consuming. This is why the issue of the thermodynamic stability of AuO in a broad pressure range will be discussed in a separate contribution, together with many other stoichiometries in the Au/O phase diagram.

■ ASSOCIATED CONTENT

Supporting Information

The Supporting Information is available free of charge on the ACS Publications website at DOI: 10.1021/acs.inorgchem.5b02528.

Crystallographic data of AuO structural candidates, electronic band structures and DOS, structures along B1−B2 transition paths, and C2/*c* AuO zone center phonon frequencies (PDF)

■ AUTHOR INFORMATION

Corresponding Authors

*E-mail: a.hermann@ed.ac.uk.
*E-mail: mariana@icm.edu.pl.

Notes

The authors declare no competing financial interest.

■ ACKNOWLEDGMENTS

A.H. and R.H. are grateful for support from EFree, an Energy Frontier Research Center, funded by the U.S. Department of Energy (Grant DESC0001057 at Cornell University), and from the U.S. National Science Foundation (Grant CHE-0910623). W.G. and M.D. acknowledge financial support from the Polish National Science Centre (NCN; Project HP 2012/06/M/ST5/00344). Computational resources provided by the Cornell NanoScale Facility (supported by the National Science Foundation through Grant ECS-0335765), the XSEDE network (provided by the National Center for Supercomputer Applications through Grant TG-DMR060055N), the KAUST Supercomputing Laboratory (Project ID k128), and the UK National Supercomputing Service (ARCHER Project ID d56) are gratefully acknowledged. Calculations at University of Warsaw were performed on ICM machines within Project G29-3.

■ REFERENCES

(1) Shi, H.; Asahi, R.; Stampfl, C. *Phys. Rev. B: Condens. Matter Mater. Phys.* **2007**, *75*, 205125.
(2) Grochala, W.; Mazej, Z. *Philos. Trans. R. Soc., A* **2015**, *373*, 20140179−20140179.
(3) Cotton, F. A.; Wilkinson, G.; Murillo, C. A.; Bochmann, M. *Advanced Inorganic Chemistry*, 6th ed.; John Wiley & Sons Inc.: New York, 1999.
(4) Steiner, P.; Hüfner, S.; Kinsinger, V.; Sander, I.; Siegwart, B.; Schmitt, H.; Schulz, R.; Junk, S.; Schwitzgebel, G.; Gold, A.; Politis, C.; Müller, H. P.; Hoppe, R.; Kemmler-Sack, S.; Kunz, C. *Z. Phys. B: Condens. Matter* **1988**, *69*, 449−458.
(5) Burdett, J. K.; Kulkarni, G. V. *Phys. Rev. B: Condens. Matter Mater. Phys.* **1989**, *40*, 8908−8932.
(6) Gao, L.; Xue, Y. Y.; Chen, F.; Xiong, Q.; Meng, R. L.; Ramirez, D.; Chu, C. W.; Eggert, J. H.; Mao, H.-K. *Phys. Rev. B: Condens. Matter Mater. Phys.* **1994**, *50*, 4260−4263.
(7) Kresse, G.; Furthmüller, J. *Phys. Rev. B: Condens. Matter Mater. Phys.* **1996**, *54*, 11169−11186.
(8) Kresse, G.; Joubert, D. *Phys. Rev. B: Condens. Matter Mater. Phys.* **1999**, *59*, 1758−1775.
(9) Blöchl, P. E. *Phys. Rev. B: Condens. Matter Mater. Phys.* **1994**, *50*, 17953−17979.
(10) Perdew, J. P.; Burke, K.; Ernzerhof, M. *Phys. Rev. Lett.* **1996**, *77*, 3865−3868.
(11) Perdew, J.; Ruzsinszky, A.; Csonka, G. I.; Vydrov, O. A.; Scuseria, G. E.; Constantin, L. A.; Zhou, X.; Burke, K. *Phys. Rev. Lett.* **2008**, *100*, 136406.
(12) Heyd, J.; Scuseria, G. E.; Ernzerhof, M. *J. Chem. Phys.* **2006**, *124*, 219906.
(13) Lonie, D. C.; Zurek, E. *Comput. Phys. Commun.* **2011**, *182*, 372−387.
(14) Zurek, E.; Hoffmann, R.; Ashcroft, N. W.; Oganov, A. R.; Lyakhov, A. O. *Proc. Natl. Acad. Sci. U. S. A.* **2009**, *106*, 17640−3.
(15) Hermann, A.; Ashcroft, N. W.; Hoffmann, R. *Proc. Natl. Acad. Sci. U. S. A.* **2012**, *109*, 745−750.
(16) Hermann, A.; Ashcroft, N. W.; Hoffmann, R. *J. Chem. Phys.* **2014**, *141*, 024505.
(17) Hermann, A.; Schwerdtfeger, P. *J. Phys. Chem. Lett.* **2014**, *5*, 4336−4342.
(18) Hermann, A.; Ashcroft, N. W.; Hoffmann, R. *Inorg. Chem.* **2012**, *51*, 9066−75.
(19) Haas, P.; Tran, F.; Blaha, P. *Phys. Rev. B: Condens. Matter Mater. Phys.* **2009**, *79*, 085104.
(20) Csonka, G. I.; Perdew, J. P.; Ruzsinszky, A.; Philipsen, P. H. T.; Lebègue, S.; Paier, J.; Vydrov, O. A.; Ángyán, J. G. *Phys. Rev. B: Condens. Matter Mater. Phys.* **2009**, *79*, 1−14.
(21) Scherbaum, F.; Grohmann, A.; Huber, B.; Krüger, C.; Schmidbaur, H. *Angew. Chem., Int. Ed. Engl.* **1988**, *27*, 1544−1546.
(22) Schmidbaur, H. *Gold Bull.* **2000**, *33*, 3−10.
(23) Pyykkö, P. *Chem. Rev.* **1997**, *97*, 597−636.
(24) Niggli, P. *Z. Kristallogr. - Cryst. Mater.* **1922**, *57*, 253−299.
(25) Tunell, G.; Posnjak, E.; Ksanda, C. J. *Z. Kristallogr. - Cryst. Mater.* **1935**, *90*, 120−142.
(26) Derzsi, M.; Hermann, A.; Hoffmann, R.; Grochala, W. *Eur. J. Inorg. Chem.* **2013**, *2013*, 5094−5102.
(27) Keinan, S.; Avnir, D. *Inorg. Chem.* **2001**, *40*, 318−23.
(28) Smith, D. W. *Coord. Chem. Rev.* **1976**, *21*, 93−158.
(29) Levi, G. R.; Fontana, C. *Gazz. Chim. Ital.* **1926**, *56*, 388−396.
(30) Moore, W. J.; Pauling, L. *J. Am. Chem. Soc.* **1941**, *63*, 1392−1394.
(31) McMillan, J. A. *J. Inorg. Nucl. Chem.* **1960**, *13*, 28−31.
(32) Brese, N. E.; O'Keeffe, M.; Ramakrishna, B. L.; Von Dreele, R. B. *J. Solid State Chem.* **1990**, *89*, 184−190.
(33) Derzsi, M.; Piekarz, P.; Grochala, W. *Phys. Rev. Lett.* **2014**, *113*, 025505.
(34) Lawton, S. L.; Rohrbaugh, W. J.; Kokotailo, G. T. *Inorg. Chem.* **1972**, *11*, 2227−2233.
(35) Dedieu, A.; Hoffmann, R. *J. Am. Chem. Soc.* **1978**, *100*, 2074−2079.
(36) Thorn, D. L.; Hoffmann, R. *J. Am. Chem. Soc.* **1978**, *100*, 2079−2090.
(37) Jiang, Y.; Alvarez, S.; Hoffmann, R. *Inorg. Chem.* **1985**, *24*, 749−757.
(38) Burdett, J. K.; Eisenstein, O.; Schweizer, W. B. *Inorg. Chem.* **1994**, *33*, 3261−3268.
(39) Pyykkö, P.; Zhao, Y. *Angew. Chem., Int. Ed. Engl.* **1991**, *30*, 604−605.
(40) Pyykkö, P. *Angew. Chem., Int. Ed.* **2004**, *43*, 4412−56.
(41) Doll, K.; Pyykkö, P.; Stoll, H. *J. Chem. Phys.* **1998**, *109*, 2339.
(42) Allen, J. P.; Scanlon, D. O.; Watson, G. W. *Phys. Rev. B: Condens. Matter Mater. Phys.* **2010**, *81*, 161103.
(43) Włodarska, I.; Derzsi, M.; Grochala, W. *Phys. Status Solidi RRL* **2015**, *9*, 401−404.
(44) Barrett, C. S.; Meyer, L.; Wasserman, J. *J. Chem. Phys.* **1967**, *47*, 592−597.

DOI: 10.1021/acs.inorgchem.5b02528
Inorg. Chem. 2016, 55, 1278−1286

(45) Neaton, J. B.; Ashcroft, N. W. *Phys. Rev. Lett.* **2002**, *88*, 205503.
(46) Wickleder, M. S. *Z. Anorg. Allg. Chem.* **2001**, *627*, 2112.
(47) Westrik, R. *Acta Crystallogr.* **1954**, *7*, 764−767.
(48) Pascard, R.; Pascard-Billy, C. *Acta Crystallogr.* **1965**, *18*, 830−834.
(49) Bader, R. F. W. *Atoms in Molecules: A Quantum Theory*; Oxford University Press: Oxford, U.K., 1994.
(50) Jarchow, O.; Schulz, H.; Nast, R. *Angew. Chem., Int. Ed. Engl.* **1970**, *9*, 71−71.
(51) Goggin, P. L.; Goodfellow, R. J. *J. Chem. Soc., Dalton Trans.* **1973**, 2355.
(52) Doonan, D. J.; Balch, A. L.; Goldberg, S. Z.; Eisenberg, R.; Miller, J. S. *J. Am. Chem. Soc.* **1975**, *97*, 1961−1962.
(53) Xu, Q.; Heaton, B. T.; Jacob, C.; Mogi, K.; Ichihashi, Y.; Souma, Y.; Kanamori, K.; Eguchi, T. *J. Am. Chem. Soc.* **2000**, *122*, 6862−6870.
(54) Holloway, R. G.; Penfold, B. R.; Colton, R.; McCormick, M. J. *J. Chem. Soc., Chem. Commun.* **1976**, 485.
(55) Brown, M. P.; Puddephatt, R. J.; Rashidi, M.; Manojlović-Muir, L.; Muir, K. W.; Solomun, T.; Seddon, K. R. *Inorg. Chim. Acta* **1977**, *23*, L33−L34.
(56) Miedaner, A.; DuBois, D. L. *Inorg. Chem.* **1988**, *27*, 2479−2484.
(57) Hoffman, D. M.; Hoffmann, R. *Inorg. Chem.* **1981**, *20*, 3543−3555.
(58) Vegas, A.; Jansen, M. *Acta Crystallogr., Sect. B: Struct. Sci.* **2002**, *58*, 38−51.
(59) Buerger, M. J. In *Phase Transformations in Solids*; Smoluchowski, R., Mayer, J. E., Weyl, W. A., Eds.; John Wiley & Sons Inc.: New York, 1951; pp 183−211.
(60) Watanabe, M.; Tokonami, M.; Morimoto, N. *Acta Crystallogr., Sect. A: Cryst. Phys., Diffr., Theor. Gen. Crystallogr.* **1977**, *33*, 294−298.
(61) Tolédano, P.; Knorr, K.; Ehm, L.; Depmeier, W. *Phys. Rev. B: Condens. Matter Mater. Phys.* **2003**, *67*, 144106.
(62) Einstein, F. W. B.; Rao, P. R.; Trotter, J.; Bartlett, N. *J. Chem. Soc. A* **1967**, 478.
(63) Seidel, S.; Seppelt, K. *Science (Washington, DC, U. S.)* **2000**, *290*, 117−118.
(64) Pearson, R. G. *Acc. Chem. Res.* **1993**, *26*, 250−255.
(65) Shimizu, K.; Suhara, K.; Ikumo, M.; Eremets, M. I.; Amaya, K. *Nature* **1998**, *393*, 767.
(66) Zurek, E.; Grochala, W. *Phys. Chem. Chem. Phys.* **2015**, *17*, 2917−2934.
(67) As derived from average Au(II)−Xe distance of 2.73 Å in $[AuXe_4](Sb_2F_{11})_2$, and covalent radius of Xe atom, 1.40 Å.
(68) Riedel, S.; Kaupp, M. *Inorg. Chem.* **2006**, *45*, 1228−1234.
(69) Pyykkö, P. *Chem. Soc. Rev.* **2008**, *37*, 1967−97.
(70) Lee, H. M.; Lee, K. H.; Lee, G.; Kim, K. S. *J. Phys. Chem. C* **2015**, *119* (25), 14383−14391, DOI: 10.1021/acs.jpcc.5b03051.
(71) Citra, A.; Andrews, L. *J. Mol. Struct.: THEOCHEM* **1999**, *489*, 95−108.
(72) Kurzydłowski, D.; Grochala, W. *Chem. Commun.* **2008**, *1*, 1073.

DOI: 10.1021/acs.inorgchem.5b02528
Inorg. Chem. 2016, 55, 1278−1286